ARTICLE

doi:10.1038/nature15709

Ion channels enable electrical communication in bacterial communities

Arthur Prindle[1], Jintao Liu[1]*, Munehiro Asally[2]*, San Ly[1], Jordi Garcia-Ojalvo[3] & Gürol M. Süel[1]

The study of bacterial ion channels has provided fundamental insights into the structural basis of neuronal signalling; however, the native role of ion channels in bacteria has remained elusive. Here we show that ion channels conduct long-range electrical signals within bacterial biofilm communities through spatially propagating waves of potassium. These waves result from a positive feedback loop, in which a metabolic trigger induces release of intracellular potassium, which in turn depolarizes neighbouring cells. Propagating through the biofilm, this wave of depolarization coordinates metabolic states among cells in the interior and periphery of the biofilm. Deletion of the potassium channel abolishes this response. As predicted by a mathematical model, we further show that spatial propagation can be hindered by specific genetic perturbations to potassium channel gating. Together, these results demonstrate a function for ion channels in bacterial biofilms, and provide a prokaryotic paradigm for active, long-range electrical signalling in cellular communities.

Communication through electrical signalling is prevalent among biological systems, with one of the most familiar examples being the action potential in neurons that is mediated by ion channels[1]. For many years, the study of bacterial ion channels has provided fundamental insights into the structural basis of such neuronal signalling[2,3]. In particular, the prokaryotic potassium ion channel KcsA provided the first structural information on ion selectivity and conductance[4]. More recently, it has been shown that bacteria possess many important classes of other ion channels, such as sodium channels[5], chloride channels[6], calcium-gated potassium channels[7] and ionotropic glutamate receptors[8], similar to those found in neurons. However, the native role of these ion channels in bacteria has largely remained unclear[9,10]. Efforts to uncover ion channel function in bacteria have identified roles in the extreme acid resistance response[6] and in osmoregulation[11], yet ion-specific channels do not appear to be solely responsible for these cellular processes. It remains unclear whether ion channels can support other unique functions in prokaryotes. We hypothesized that studying bacteria in their native context, the biofilm community, may reveal new clues about the function of ion channels in bacteria.

Bacterial biofilms are organized communities containing billions of densely packed cells. Such communities can exhibit fascinating macroscopic spatial coordination[12–17]. However, it remains unclear how microscopic bacteria can communicate effectively over large distances. To investigate this question, we studied a *Bacillus subtilis* microbial community that was recently reported to undergo metabolic oscillations triggered by nutrient limitation[18]. The oscillatory dynamics resulted from long-range metabolic co-dependence between cells in the interior and periphery of the biofilm (Fig. 1a)[18]. Specifically, interior and peripheral cells compete for glutamate, while sharing ammonium. As a result, biofilm growth halts periodically, increasing nutrient availability for the sheltered interior cells. Interestingly, glutamate (Glu^-) and ammonium (NH_4^+) are both charged metabolites, whose respective uptake and retention is known to depend on the transmembrane electrical potential and proton motive force[19,20]. Therefore, we wondered whether metabolic coordination among distant cells within the biofilm might also involve a form of electrochemical signalling.

Oscillations in membrane potential

To monitor long-range electrical fluctuations in the bacterial community as a function of space and time, we grew biofilms in an unconventionally large microfluidic device (Fig. 1b and 'Microfluidics' section of Methods). To measure electrical signalling, we used the fluorescent cationic dye thioflavin T (ThT) to quantify membrane potential within the biofilm. ThT is positively charged and can be retained in cells because of the negative electrical membrane potential inside cells. Thus, cells with a negative membrane potential will retain more ThT, allowing it to act as a Nernstian voltage indicator[21,22]. We confirmed that ThT faithfully reports the membrane potential by comparing it to an established reporter of membrane potential in bacteria[23], 3,3′-dipropylthiadicarbocyanine iodide ($DiSC_3(5)$) (Extended Data Fig. 1a). We found that ThT has an approximately threefold higher sensitivity to changes in membrane potential compared to $DiSC_3(5)$ (Extended Data Fig. 1a, inset). Furthermore, we exposed cells to minor changes in external pH, which is known to alter membrane potential[24], and observed the expected changes in ThT (Extended Data Fig. 1b). Therefore, ThT accurately reports on changes in membrane potential for bacteria residing in biofilms.

We next investigated changes in membrane potential during metabolic oscillations. In particular, quantitative measurements of ThT fluorescence showed global and self-sustained oscillations consistent with the reported period of the metabolic oscillations (Fig. 1c, Supplementary Video 1 and Extended Data Fig. 1c)[18]. Furthermore, oscillations in ThT could be quenched by supplementation of the media with glutamine, which bypasses the need for glutamate and ammonium (Extended Data Fig. 1d). These data show a connection between metabolic oscillations and membrane potential. Notably, oscillations in membrane potential were synchronized among even the most distant regions of the biofilm community (Fig. 1d, e). We wondered whether active electrochemical signalling could be responsible for this long-range synchronization.

[1]Division of Biological Sciences, University of California San Diego, California 92093, USA. [2]Warwick Integrative Synthetic Biology Centre, School of Life Sciences, University of Warwick, Coventry CV4 7AL, UK. [3]Department of Experimental and Health Sciences, Universitat Pompeu Fabra, 08003 Barcelona, Spain.
*These authors contributed equally to this work.

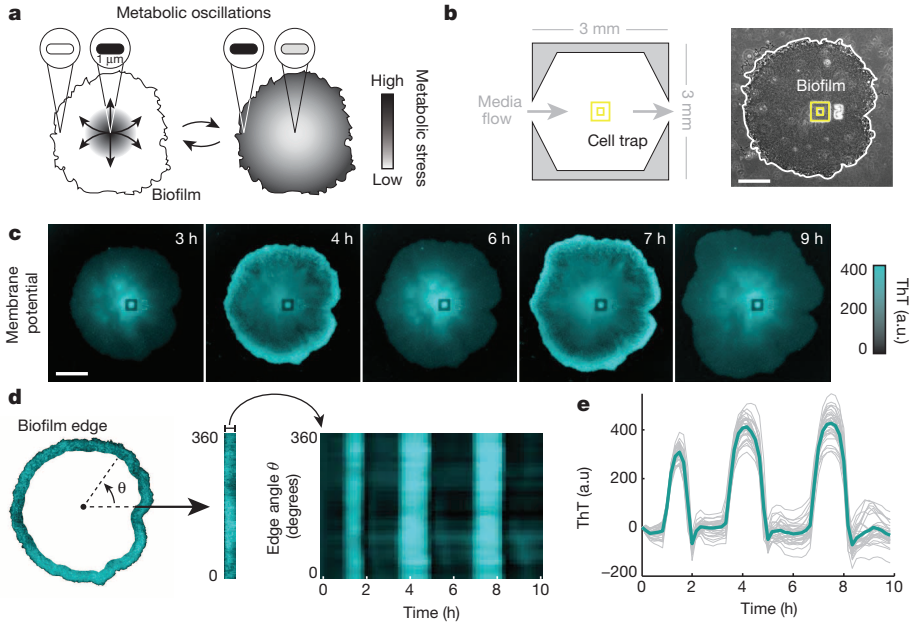

Figure 1 | Biofilms produce synchronized oscillations in membrane potential. **a**, Biofilms generate collective metabolic oscillations resulting from long-range metabolic interactions between interior and peripheral cells[18]. It remains unclear how microscopic bacteria are capable of communicating over such macroscopic distances within biofilm communities. **b**, Schematic of the microfluidic device used throughout this study (left). Phase contrast image of a biofilm growing in the microfluidic device with the cell trap highlighted in yellow (right). Scale bar, 100 μm. **c**, Global oscillations in membrane potential, as reported by thioflavin T (ThT), within the biofilm community. ThT is positively charged but not known to be actively transported, so it can be retained in cells due to their negative membrane potential inside the cell. ThT fluorescence increases when the inside of the cell becomes more negative, and thus ThT is inversely related to the membrane potential. Scale bar, 0.15 mm. Representative images shown are taken from over 75 independent biofilms. a.u., arbitrary units. **d**, Membrane potential oscillations are highly synchronized even between the most distant regions of the biofilm. To analyse synchronization, the edge region of the biofilm was identified and straightened (left) then plotted over time (right). **e**, Time traces of the heat map shown in **d**. Indicated in bold is the mean of 30 traces.

Active propagation of potassium signal

Changes in membrane potential involve the movement of charged species across the cellular membrane. We suspected the involvement of potassium, since it is the most abundant cation in all living cells[25] and has been implicated to have a role in biofilm formation[26,27]. *B. subtilis* uses active potassium transport mechanisms to concentrate intracellular potassium at approximately 300 mM[28–30]. This intracellular concentration is nearly 40 times the external media concentration. Consequently, sudden release of this potassium gradient would increase extracellular potassium concentration and generate a change in the membrane potential. Accordingly, we used a fluorescent chemical potassium dye, asante potassium green-4 (APG-4[31]), to measure the extracellular concentration of potassium in the biofilm (Fig. 2a and Extended Data Fig. 2a, b). We observed global oscillations in APG-4 that correlated with membrane potential, which suggests that the membrane potential oscillations could involve the release of potassium (Fig. 2b, c and Supplementary Video 2). In agreement with this finding, oscillations in extracellular potassium extended beyond the biofilm to the surrounding growth media (Extended Data Fig. 2c). We also measured the dynamics of sodium, another ion commonly used by cells to modulate membrane potential, and observed no oscillations (Extended Data Fig. 2d–f). Together, these data suggest that potassium has a role in the synchronized oscillations in membrane potential.

Furthermore, we directly tested that oscillations in membrane potential were driven by flow of potassium across the cell membrane. Specifically, we clamped net potassium flux across the cell membrane by supplementing the growth media with 300 mM KCl (matching the intracellular potassium concentration) (Fig. 2d). When we applied this chemical potassium clamp, oscillations in membrane potential abruptly halted (Fig. 2e). Applying this clamp together with valinomycin, a potassium ionophore that acts as potassium-specific carrier in the cellular membrane[32], yielded a similar quenching of oscillations (Extended Data Fig. 3a, b). Therefore, changes in the electrochemical potential for potassium appear to be required for the observed oscillations in membrane potential.

Next, we determined whether cells could actively propagate the extracellular potassium signal through the biofilm to sustain long-range communication. While diffusive signals decay over space and time, active signalling processes can amplify the signal, avoiding such decay (Fig. 2f). To determine which of these processes may be operating in the biofilm, we observed the propagation of the extracellular potassium signal (Fig. 2g). Results show that the signal travels at a constant rate of propagation (Extended Data Fig. 3c, d). Furthermore, the amplitude of the signal does not decay with distance travelled, in contrast to what is predicted for passive potassium diffusion (Fig. 2h). These findings are consistent with a process in which cells actively propagate the potassium signal. Together, these results suggest that the biofilm synchronizes global oscillations in membrane potential by an active signalling process involving potassium ions.

Potassium ion-channel-mediated signalling

Motivated by our findings, we explored the role of ion channels in the observed potassium signalling. We focused on YugO, the only experimentally described potassium channel in *B. subtilis*, which is also reported to be important for biofilm formation[33]. Potassium flux through YugO is gated by an intracellular TrkA domain, known to be regulated by the metabolic state of the cell[34–36]. Accordingly, we hypothesized that metabolic limitation could form the initial trigger for YugO activation. Specifically, since glutamate limitation is known to drive the underlying metabolic oscillations[18], we anticipated that transient removal of glutamate could initiate potassium release. To test this, we transiently deprived cells of glutamate and measured extracellular potassium in both wild-type and *yugO* deletion strains (see 'Strains' section of the Methods). As expected, we observed extracellular potassium increase for wild-type but not the *yugO* deletion

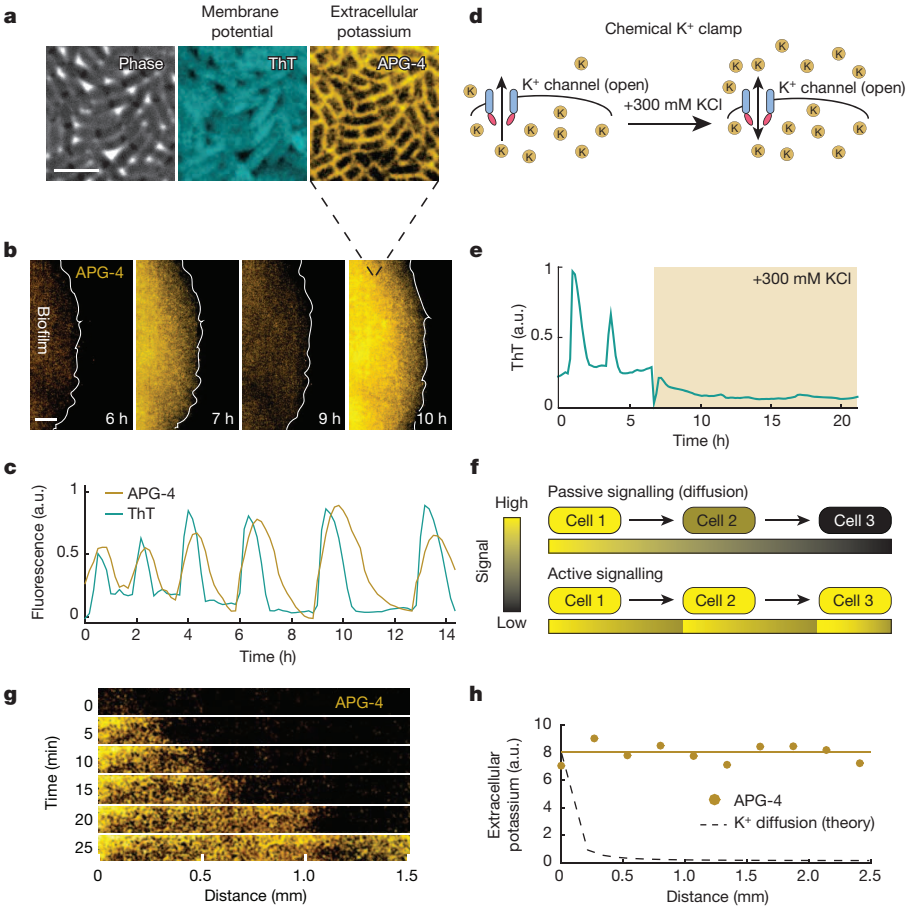

Figure 2 | Potassium release is involved in active signal propagation within the biofilm. **a**, An extracellular fluorescent chemical dye (APG-4) reports the concentration of potassium in the media (Extended Data Fig. 2a, b). For comparison, the same cells are shown stained with ThT, which is inversely related to the membrane potential. These images depict cells at the peak of the ThT oscillation cycle. Representative images are selected from six independent experiments. Scale bar, 2 μm. **b**, Global oscillations in extracellular potassium throughout the biofilm. A white line indicates the edge of the biofilm. Representative images are selected from six independent experiments. Scale bar, 0.2 mm. **c**, Oscillations in membrane potential and extracellular potassium are synchronized, suggesting that potassium release is involved in global membrane potential oscillations. ThT is inversely related to the membrane potential. Representative traces are taken from the experiment shown in **b**. **d**, A chemical potassium clamp (300 mM KCl, matching the intracellular concentration[29]) prevents the formation of potassium electrochemical gradients across the cellular membrane. **e**, Clamping net potassium flux quenches oscillations in membrane potential. Representative trace is selected from two independent experiments. **f**, Illustration of the differences between passive signalling (diffusion) and active signalling. When cells passively respond to a signal, the range that the signal can propagate is limited due to the decay of signal amplitude. In contrast, when cells actively respond by amplifying the signal, propagation can extend over greater distances. **g**, We measured propagation of extracellular potassium by measuring APG-4 in time and along a length of approximately 1.5 mm within the biofilm. **h**, Extracellular potassium amplitude is relatively constant as the signal propagates, in contrast to the predicted amplitude decay of a passive signal. Representative data selected from six independent experiments. The diffusion line is calculated using the 2D diffusion equation and the diffusion coefficient for potassium within biofilms (Supplementary Information).

strain (Fig. 3a). These findings suggest that glutamate limitation can trigger the potassium signal via the YugO potassium channel.

Next, we investigated whether YugO also has a role in the active propagation of the potassium signal. To test this, we measured the response of wild-type and *yugO* deletion strains to transient bursts of external potassium (300 mM KCl). As expected, potassium exposure first resulted in a short-term membrane potential depolarization in both strains. However, in the wild-type strain this initial depolarization was typically followed by an extended hyperpolarization phase, which was not observed in the *yugO* deletion strain (Fig. 3b). This period of hyperpolarization was accompanied by an increase in extracellular potassium (Extended Data Fig. 4a). Together, these data indicate that potassium exposure triggers a release of intracellular potassium through YugO. Exposure to an equivalent concentration of sorbitol (an uncharged solute) did not elicit an equivalent response, ruling out purely osmotic effects (Extended Data Fig. 4b). Therefore, YugO appears to have a role in propagating the extracellular potassium signal within the biofilm.

Mathematical modelling of electrical signalling

Our data thus point to a proposed mechanism where metabolically stressed cells release intracellular potassium, and the resulting elevated extracellular potassium imposes further metabolic stress onto neighbouring cells (Fig. 3c). In *B. subtilis*, glutamate is co-transported with two protons by the GltP transporter and this process depends on the proton motive force[19]. Potassium-mediated depolarization of the membrane potential can transiently reduce the electrical component of the proton motive force[24], and thereby lower glutamate uptake and intracellular ammonium retention[19,20]. Therefore, potassium-mediated signalling could propagate metabolic stress onto distant cells (Fig. 3c, right). Accordingly, hyperpolarization triggered by YugO activation may represent a cellular response to enhance glutamate uptake or ammonium retention. This notion is supported by our finding that the response to extracellular potassium can be abolished by growing cells in glutamine, an uncharged metabolite and preferred nitrogen source that bypasses the need for glutamate and ammonium[37] (Extended Data Fig. 4c). This result further supports the

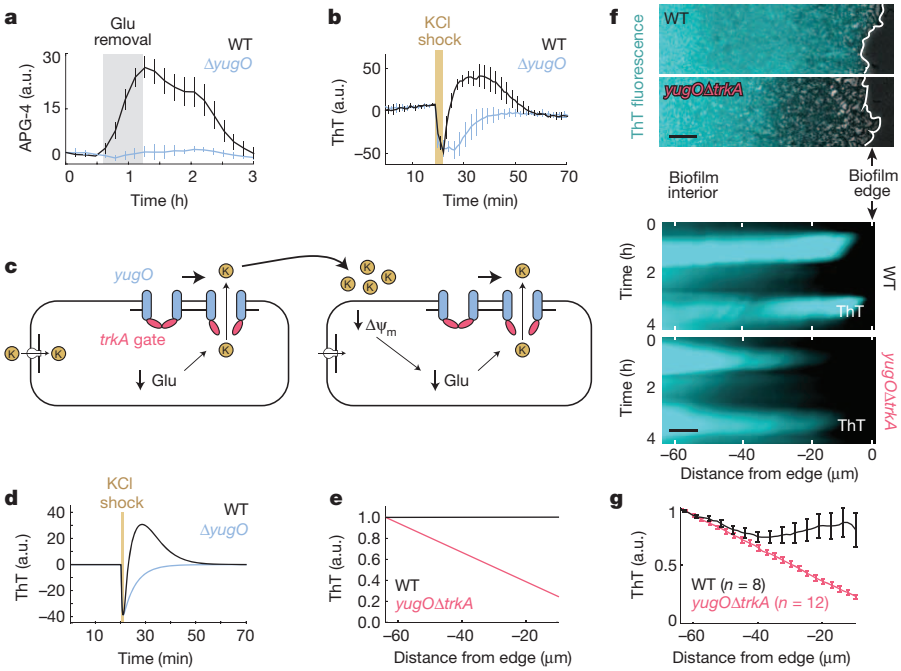

Figure 3 | The molecular mechanism of signal propagation involves potassium channel gating. **a**, *yugO* is a potassium channel in *B. subtilis* that is gated intracellularly by a *trkA* domain, which is regulated by the metabolic state of the cell[34–36]. Withdrawing glutamate (the sole nitrogen source in MSgg media) induces an increase in extracellular potassium (APG-4) for wild-type (WT) but not the *yugO* deletion strain. Error bars indicate the mean ± s.d. for three independent biofilms each. **b**, An external potassium shock (300 mM KCl) induces a short-term membrane potential depolarization in both wild-type and *yugO* deletion strains. However, in the wild type this initial depolarization was followed by hyperpolarization, which is not observed in the *yugO* deletion strain (mean ± s.d. for 12 traces drawn from 3 biofilms each). ThT is inversely related to the membrane potential. **c**, Proposed model for potassium signalling. The initial trigger for potassium release is metabolic stress caused by glutamate limitation. External potassium depolarizes neighbouring cells, producing further nitrogen limitation by limiting glutamate uptake, and thus produces further metabolic stress. This cycle results in cell–cell propagation of the potassium signal. **d**, A minimal conductance-based model describing the dynamics of the cell's membrane potential in terms of a single potassium channel and a leak current. Consistent with our experimental results, this simple model exhibits transient depolarization followed by hyperpolarization in response to local increases in extracellular potassium concentration. **e**, The model predicts that manipulating channel gating and conductance will result in decaying amplitude in the spatial propagation of membrane potential oscillations. **f**, Maximum intensity projection of membrane potential change illustrating attenuated communication within the biofilm in a *yugOΔtrkA* deletion compared to wild-type biofilms (top). Heat map of oscillations taken from wild-type and *yugOΔtrkA* mutant biofilms (bottom). Representative images are taken from three independent biofilm experiments in which wild-type and *yugOΔtrkA* biofilms are compared head-to-head. Scale bars, 8 μm. **g**, Quantification of normalized pulse amplitude from wild-type ($n = 8$ pulses) and *yugOΔtrkA* ($n = 12$ pulses) mutant biofilms (mean ± s.e.m.).

specific link between potassium-mediated electrical signalling and metabolic stress.

To determine whether the proposed potassium-channel-based mechanism is sufficient to account for the observed propagating pulses of electrical activity, we turned to mathematical modelling. Specifically, we considered a minimal conductance-based model describing the dynamics of the cell's membrane potential in terms of a single potassium channel and a leak current (see 'Mathematical Model' section of the Supplementary Information). Consistent with our experimental results, this simple model exhibits transient depolarization followed by hyperpolarization in response to local increases in extracellular potassium concentration (Fig. 3d). Furthermore, the model shows long-range propagation of these excitations without decay in the amplitude of membrane potential oscillations (Fig. 3e). Therefore, the proposed mechanism is mathematically sufficient to qualitatively account for the observed membrane potential dynamics and active propagation in space.

The model also predicts that reduced efficiency of the potassium channel function could lead to degradation in long-range communication (Fig. 3e). Since a complete *yugO* deletion interferes with development of large biofilms[33], we constructed a strain in which we deleted the TrkA gating domain, leaving only the ion channel portion of YugO intact (see 'Strains' section of the Methods). Similarly truncated bacterial potassium channels have been shown to have altered gating and ion conductance[34,38]. Indeed, the *yugOΔtrkA* mutant biofilms exhibited a reduced propagation of membrane potential oscillations (Fig. 3f and Supplementary Video 3). Specifically, in contrast to wild type, the *yugOΔtrkA* mutant shows decay in the signal amplitude from the interior of the biofilm to the cells at the periphery, which is also consistent with model predictions (Fig. 3g). Thus, YugO channel gating appears to promote efficient electrical communication between distant cells.

Discussion

Our findings suggest that bacteria use potassium ion-channel-mediated electrical signals to coordinate metabolism within the biofilm. The ensuing 'bucket brigade' of potassium release allows cells to rapidly communicate their metabolic state, taking advantage of a link between membrane potential and metabolic activity. This form of electrical communication can thus enhance the previously described long-range metabolic co-dependence in biofilms[18]. Specifically, the wave of depolarization triggered by metabolically stressed interior cells would limit the ability of cells in the biofilm periphery to take up glutamate or retain ammonium, thereby allowing interior cells more access to these nutrients. This also provides a possible explanation for the observation that the *yugO* deletion strain has a defect in biofilm development[33]. Interestingly, owing to the rapid diffusivity of potassium ions in aqueous environments, it is also conceivable that even physically disconnected biofilms could be capable of synchronizing their metabolic oscillations by a similar exchange of potassium ions.

The role of ion-channel-mediated electrical communication has long been appreciated[39]. While cation channels are found in all organisms[9,10]

and potassium is the dominant intracellular cation[25], electrical signalling is commonly viewed to be a property of neurons. However, several recent studies have suggested that in addition to traditional cell-to-cell communication systems such as quorum sensing[40], bacteria may use electron flux[41–43] to communicate. The herein described study of electrical coordination of metabolism in microbial communities may in turn hold some general insights that extend beyond bacteria. For example, the connection between neuronal signalling and metabolic activity (neurometabolism) is an active area of research[44,45]. Furthermore, depletion of glutamate, the most common excitatory neurotransmitter[46], also forms the initial trigger for these collective metabolic oscillations synchronized by potassium. Therefore, it is intriguing to think not only about the structural similarities between bacterial and human potassium ion channels[2,3], but also their possible functional similarities with respect to long-range electrical communication.

Online Content Methods, along with any additional Extended Data display items and Source Data, are available in the online version of the paper; references unique to these sections appear only in the online paper.

Received 16 June; accepted 10 September 2015.

Published online 21 October 2015.

1. Gerstner, W. & Kistler, W. M. *Spiking Neuron Models: Single Neurons, Populations, Plasticity* (Cambridge Univ. Press, 2002).
2. Hille, B. *Ion Channels of Excitable Membranes* (Sinauer Associates, 2001).
3. MacKinnon, R. Potassium channels and the atomic basis of selective ion conduction. *Biosci. Rep.* **24,** 75–100 (2004).
4. Doyle, D. A. *et al.* The structure of the potassium channel: molecular basis of K^+ conduction and selectivity. *Science* **280,** 69–77 (1998).
5. Ren, D. *et al.* A prokaryotic voltage-gated sodium channel. *Science* **294,** 2372–2375 (2001).
6. Iyer, R., Iverson, T. M., Accardi, A. & Miller, C. A biological role for prokaryotic ClC chloride channels. *Nature* **419,** 715–718 (2002).
7. Jiang, Y. *et al.* Crystal structure and mechanism of a calcium-gated potassium channel. *Nature* **417,** 515–522 (2002).
8. Chen, G. Q., Cui, C., Mayer, M. L. & Gouaux, E. Functional characterization of a potassium-selective prokaryotic glutamate receptor. *Nature* **402,** 817–821 (1999).
9. Kuo, M. M. C., Haynes, W. J., Loukin, S. H., Kung, C. & Saimi, Y. Prokaryotic K^+ channels: From crystal structures to diversity. *FEMS Microbiol. Rev.* **29,** 961–985 (2005).
10. Saimi, Y., Loukin, S. H., Zhou, X. L., Martinac, B. & Kung, C. Ion channels in microbes. *Methods Enzymol.* **294,** 507–524 (1998).
11. Martinac, B., Buechner, M., Delcour, A. H., Adler, J. & Kung, C. Pressure-sensitive ion channel in *Escherichia coli*. *Proc. Natl Acad. Sci. USA* **84,** 2297–2301 (1987).
12. Costerton, J. W., Stewart, P. S. & Greenberg, E. P. Bacterial biofilms: a common cause of persistent infections. *Science* **284,** 1318–1322 (1999).
13. Hall-Stoodley, L., Costerton, J. W. & Stoodley, P. Bacterial biofilms: from the natural environment to infectious diseases. *Nature Rev. Microbiol.* **2,** 95–108 (2004).
14. Vlamakis, H., Aguilar, C., Losick, R. & Kolter, R. Control of cell fate by the formation of an architecturally complex bacterial community. *Genes Dev.* **22,** 945–953 (2008).
15. Asally, M. *et al.* Localized cell death focuses mechanical forces during 3D patterning in a biofilm. *Proc. Natl Acad. Sci. USA* **109,** 18891–18896 (2012).
16. Wilking, J. N. *et al.* Liquid transport facilitated by channels in *Bacillus subtilis* biofilms. *Proc. Natl Acad. Sci. USA* **110,** 848–852 (2013).
17. Payne, S. *et al.* Temporal control of self-organized pattern formation without morphogen gradients in bacteria. *Mol. Syst. Biol.* **9,** 697 (2013).
18. Liu, J. *et al.* Metabolic co-dependence gives rise to collective oscillations within microbial communities. *Nature* **523,** 550–554 (2015).
19. Tolner, B., Ubbink-Kok, T., Poolman, B. & Konings, W. N. Characterization of the proton/glutamate symport protein of *Bacillus subtilis* and its functional expression in *Escherichia coli*. *J. Bacteriol.* **177,** 2863–2869 (1995).
20. Boogerd, F. C. *et al.* AmtB-mediated NH_3 transport in prokaryotes must be active and as a consequence regulation of transport by GlnK is mandatory to limit futile cycling of NH_4^+/NH_3. *FEBS Lett.* **585,** 23–28 (2011).
21. Kralj, J. M., Hochbaum, D. R., Douglass, A. D. & Cohen, A. E. Electrical spiking in *Escherichia coli* probed with a fluorescent voltage-indicating protein. *Science* **333,** 345–348 (2011).
22. Lo, C.-J., Leake, M. C., Pilizota, T. & Berry, R. M. Nonequivalence of membrane voltage and ion-gradient as driving forces for the bacterial flagellar motor at low load. *Biophys. J.* **93,** 294–302 (2007).
23. Strahl, H. & Hamoen, L. W. Membrane potential is important for bacterial cell division. *Proc. Natl Acad. Sci. USA* **107,** 12281–12286 (2010).
24. Krulwich, T. A., Sachs, G. & Padan, E. Molecular aspects of bacterial pH sensing and homeostasis. *Nature Rev. Microbiol.* **9,** 330–343 (2011).
25. Epstein, W. The roles and regulation of potassium in bacteria. *Prog. Nucleic Acid Res. Mol. Biol.* **75,** 293–320 (2003).
26. López, D., Fischbach, M. A., Chu, F., Losick, R. & Kolter, R. Structurally diverse natural products that cause potassium leakage trigger multicellularity in *Bacillus subtilis*. *Proc. Natl Acad. Sci. USA* **106,** 280–285 (2009).
27. Kinsinger, R. F., Kearns, D. B., Hale, M. & Fall, R. Genetic requirements for potassium ion-dependent colony spreading in *Bacillus subtilis*. *J. Bacteriol.* **187,** 8462–8469 (2005).
28. Vieira-Pires, R. S., Szollosi, A. & Morais-Cabral, J. H. The structure of the KtrAB potassium transporter. *Nature* **496,** 323–328 (2013).
29. Holtmann, G., Bakker, E. P., Uozumi, N. & Bremer, E. KtrAB and KtrCD: Two K^+ uptake systems in *Bacillus subtilis* and their role in adaptation to hypertonicity. *J. Bacteriol.* **185,** 1289–1298 (2003).
30. Whatmore, A. M., Chudek, J. A. & Reed, R. H. The effects of osmotic upshock on the intracellular solute pools of *Bacillus subtilis*. *J. Gen. Microbiol.* **136,** 2527–2535 (1990).
31. Rimmele, T. S. & Chatton, J. Y. A novel optical intracellular imaging approach for potassium dynamics in astrocytes. *PLoS ONE* **9,** 1–9 (2014).
32. Margolin, Y. & Eisenbach, M. Voltage clamp effects on bacterial chemotaxis. *J. Bacteriol.* **159,** 605–610 (1984).
33. Lundberg, M. E., Becker, E. C. & Choe, S. MstX and a putative potassium channel facilitate biofilm formation in *Bacillus subtilis*. *PLoS ONE* **8,** e60993 (2013).
34. Cao, Y. *et al.* Gating of the TrkH ion channel by its associated RCK protein TrkA. *Nature* **496,** 317–322 (2013).
35. Roosild, T. P., Miller, S., Booth, I. R. & Choe, S. A mechanism of regulating transmembrane potassium flux through a ligand-mediated conformational switch. *Cell* **109,** 781–791 (2002).
36. Schlosser, A., Hamann, A., Bossemeyer, D., Schneider, E. & Bakker, E. P. NAD^+ binding to the *Escherichia coli* K^+-uptake protein TrkA and sequence similarity between TrkA and domains of a family of dehydrogenases suggest a role for NAD^+ in bacterial transport. *Mol. Microbiol.* **9,** 533–543 (1993).
37. Fisher, S. H. Regulation of nitrogen metabolism in *Bacillus subtilis*: vive la différence! *Mol. Microbiol.* **32,** 223–232 (1999).
38. Cortes, D. M., Cuello, L. G. & Perozo, E. Molecular architecture of full-length KcsA: role of cytoplasmic domains in ion permeation and activation gating. *J. Gen. Physiol.* **117,** 165–180 (2001).
39. Hodgkin, A. L. & Huxley, A. F. A quantitative description of membrane current and its applications to conduction and excitation in nerve. *J. Physiol. (Lond.)* **117,** 500–544 (1952).
40. Waters, C. M. & Bassler, B. L. Quorum sensing: cell-to-cell communication in bacteria. *Annu. Rev. Cell Dev. Biol.* **21,** 319–346 (2005).
41. Kato, S., Hashimoto, K. & Watanabe, K. Iron-oxide minerals affect extracellular electron-transfer paths of *Geobacter* spp. *Microbes Environ.* **28,** 141–148 (2013).
42. Pfeffer, C. *et al.* Filamentous bacteria transport electrons over centimetre distances. *Nature* **491,** 218–221 (2012).
43. Masi, E. *et al.* Electrical spiking in bacterial biofilms. *J. R. Soc. Interface* **12,** 1–10 (2014).
44. Pan, J. W. *et al.* Neurometabolism in human epilepsy. *Epilepsia* **49,** 31–41 (2008).
45. Petroff, O. A. C., Errante, L. D., Rothman, D. L., Kim, J. H. & Spencer, D. D. Glutamate-glutamine cycling in the epileptic human hippocampus. *Epilepsia* **43,** 703–710 (2002).
46. Meldrum, B. S. Glutamate as a neurotransmitter in the brain: review of physiology and pathology. *J. Nutr.* **130,** 1007S–1015S (2000).

Supplementary Information is available in the online version of the paper.

Acknowledgements We would like to thank S. Lockless, K. Süel, R. Wollman, T. Çağatay and M. Elowitz for comments during the writing of the manuscript, and C. Piggott for cloning help. A.P. is a Simons Foundation Fellow of the Helen Hay Whitney Foundation. J.G.-O. is supported by the Ministerio de Economia y Competitividad (Spain) and FEDER, under project FIS2012-37655-C02-01, and by the ICREA Academia Programme. This research was funded by the National Institutes of Health, National Institute of General Medical Sciences Grant R01 GM088428 and the National Science Foundation Grant MCB-1450867 50867 (both to G.M.S.). This work was also supported by the San Diego Center for Systems Biology (NIH Grant P50 GM085764).

Author Contributions G.M.S., A.P., J.L., M.A. and J.G.-O. designed the research, A.P. and J.L. performed the experiments, J.L. and A.P. performed the data analysis, J.G.O. performed the mathematical modelling, S.L. made the bacteria strains, and G.M.S., A.P., J.L. and J.G.-O. wrote the manuscript. All authors discussed the manuscript.

Author Information Reprints and permissions information is available at www.nature.com/reprints. The authors declare no competing financial interests. Readers are welcome to comment on the online version of the paper. Correspondence and requests for materials should be addressed to G.M.S. (gsuel@ucsd.edu).

METHODS

No statistical methods were used to predetermine sample size.

Strains. All experiments were done using *Bacillus subtilis* NCIB 3610. The wild-type strain was a gift from W. Winkler (University of Maryland)[47], and all other strains were derived from it and are listed in Extended Data Table 1. To make deletion strains, we used polymerase chain reaction (PCR) to amplify the desired regions from the wild-type strain. The PCR products were then put within the pER449 vector (gift from W. Winkler). For the *trkA* mutant, we deleted the C-terminal portion of *yugO* (amino acids 117–328), leaving only the N-terminal ion channel portion of *yugO* (amino acids 1–116). We identified the *trkA* region using Pfam (http://pfam.xfam.org/). All constructs were confirmed by direct sequencing and then integrated into the chromosome of the wild-type strain by a standard one-step transformation procedure[48]. Finally, chromosomal integrations were confirmed by colony PCR using the corresponding primers.

Growth conditions. The biofilms were grown in MSgg medium[16] which contains 5 mM potassium phosphate buffer (pH 7.0), 100 mM MOPS buffer (pH 7.0, adjusted using NaOH), 2 mM $MgCl_2$, 700 μM $CaCl_2$, 50 μM $MnCl_2$, 100 μM $FeCl_3$, 1 μM $ZnCl_2$, 2 μM thiamine HCl, 0.5% (v/v) glycerol and 0.5% (w/v) monosodium glutamate. The MSgg medium was made from stock solutions on the day of the experiment, and the stock solution for glutamate was newly made weekly.

Microfluidics. We followed methods similar to a previous study[18]. Briefly, we used the CellASIC ONIX Microfluidic Platform and the Y04D microfluidic plate (EMD Millipore). We used a pump pressure of 1 psi with only one media inlet open, which corresponds to a flow speed of $\sim$16 μm s^{-1}. On the day before the experiment, cells from −80 °C glycerol stock were streaked onto an LB agar plate and incubated at 37 °C overnight. The next morning, a single colony was picked from the plate and inoculated into 3 ml of LB broth and incubated in a 37 °C shaker. After 2.5 h of incubation, the cell culture was centrifuged at 2,100 relative centrifugal force (rcf) for 1 min, and the cell pellet was re-suspended in MSgg and immediately loaded into microfluidic chambers. After loading, cells in the microfluidic chamber were incubated at 37 °C for 90 min, and then the temperature was kept at 30 °C for the rest of the experiment.

Time-lapse microscopy. The growth of the biofilms was recorded using phase-contrast microscopy. The microscopes used were Olympus IX83 and DeltaVision PersonalDV. To image entire biofilms, 10 × objectives were used in most of the experiments. Biofilm phase contrast and fluorescence images were taken every 10 min, except in Fig. 2g where images were taken every 5 min. To generate Fig. 3b and Extended Data Figs 4a–c, where high temporal resolution was required, images were taken every minute. Whenever fluorescence images were recorded, we used the minimum exposure time that still provided a good signal-to-noise ratio (for example, we typically used 20 ms exposure for ThT and 100 ms exposure for APG-4).

Image analysis. Fiji/ImageJ (National Institutes of Health) and MATLAB (MathWorks) were used for image analysis. We generated custom scripts and used the image analysis toolbox to perform image segmentation on biofilm phase contrast images. To measure biofilm growth rate, we identified the biofilm area in each frame by segmenting the images and took the derivative of biofilm radius over time. We identified the radius by assuming circular growth of the colony and taking the length from the centre of the cell trap to the biofilm edge. To generate membrane potential curves, we measured the fluorescence of ThT within the biofilm using the ImageJ 'Plot Z-axis Profile' command and performed subsequent analysis, such as normalization and subtracting of baseline signal, in MATLAB.

Experimental reproducibility. Data shown in the main figures were drawn from a minimum of three independent experiments and often many more. For example, we analysed ThT oscillations (represented in Fig. 1c–e) in over 75 biofilms. In cases where only a single representative trace is shown, we analysed multiple regions within the biofilm to ensure accuracy of the analysis. In experiments comparing the wild-type and a mutant strain (*yugO* or *yugOΔtrkA*), we always performed head-to-head experiments (separate chambers in the same microfluidic device) on the same day using the same media to eliminate possible artefacts.

Mathematical modelling. The theoretical curves shown in Fig. 3d, e were generated using a mathematical model inspired by the Hodgkin–Huxley model of neuronal excitability[39] (Supplementary Information). The parameters used in the model (Extended Data Table 2) were constrained using a combination of literature values[24] and experimental data. Specifically, the response time to KCl shock (Fig. 3b) was used as a constraint on parameters with a time dimension and the spatial scale (lattice size of the 1d simulations) is extracted from the characteristic distance shown in Fig. 3g.

Theoretical estimate of potassium diffusion within biofilms. We used the diffusion coefficient of potassium in water (19.7×10^{-6} cm^2 s^{-1})[49] and reduced it to 70% in accordance with a reference on diffusion in biofilms[50], yielding the value of the diffusion coefficient (13.8×10^{-6} cm^2 s^{-1}) used in the mathematical model as well as the theoretical curves plotted alongside our experimental data. To estimate the rate of potassium propagation by diffusion, we used the formula for 2D mean squared displacement (MSD):

$$r = \sqrt{4Dt}$$

Where r is the displacement, D is the diffusion coefficient, and t is time. We used this relationship to generate the curve shown in Extended Data Fig. 3d. We directly compared the log–log slope of the experimental data (slope = 1.1, $R^2 = 0.96$) to that expected for diffusion (slope = 0.5) to further confirm that the experimental data cannot be explained by simple diffusion.

To estimate the decay of amplitude by diffusion, we used the formula for the concentration profile of 2D diffusion:

$$C(r,t) = \frac{M}{4\pi Dt}\exp\left(-\frac{r^2}{4Dt}\right)$$

Where C is the concentration of potassium at displacement r and time t, M is a constant related to the initial pulse amplitude of potassium that we matched to the initial experimental pulse amplitude of APG-4, and D is the diffusion coefficient. We used this relationship to generate the curve in Fig. 2h.

Dyes and concentrations. Thioflavin T (ThT) and $DiSC_3(5)$ were used at 10 μM. We used ThT and $DiSC_3(5)$ to track relative changes in the membrane potential, where the fluorescence of ThT increases when the cell becomes more inside negative (hyperpolarizes). We found the sensitivity of ThT to be significantly higher than that of $DiSC_3(5)$, where sensitivity is defined as the ratio between the amplitude of oscillation and its error (Extended Data Fig. 1a). Furthermore, under our experimental conditions, $DiSC_3(5)$ appears to be absorbed by the PDMS in the microfluidic device. This hinders quantitative analysis (lower sensitivity) and also greatly increases the time required for the dye to diffuse into the biofilm.

APG-4 (TEFLabs) was used at 2 μM. We used the membrane-impermeable TMA^+ salt form to track the extracellular concentration of potassium. We verified that APG-4 does not significantly diffuse into cells (Extended Data Fig. 2a). We also verified that APG-4 could measure extracellular potassium in MSgg media within our microfluidic device (Extended Data Fig. 2b).

We used ANG-2 (TEFLabs) at 2 μM. We used the membrane-impermeable TMA^+ salt form to track the extracellular concentration of sodium (Extended Data Fig. 3c, d).

47. Irnov, I. & Winkler, W. C. A regulatory RNA required for antitermination of biofilm and capsular polysaccharide operons in Bacillales. *Mol. Microbiol.* **76,** 559–575 (2010).
48. Jarmer, H., Berka, R., Knudsen, S. & Saxild, H. H. Transcriptome analysis documents induced competence of Bacillus subtilis during nitrogen limiting conditions. *FEMS Microbiol. Lett.* **206,** 197–200 (2002).
49. Horvath, A. L. *Handbook of Aqueous Electrolyte Solutions: Physical Properties, Estimation and Correlation Methods* (Ellis Horwood Ltd, 1985).
50. Stewart, P. S. Diffusion in biofilms. *J. Bacteriol.* **185,** 1485–1491 (2003).

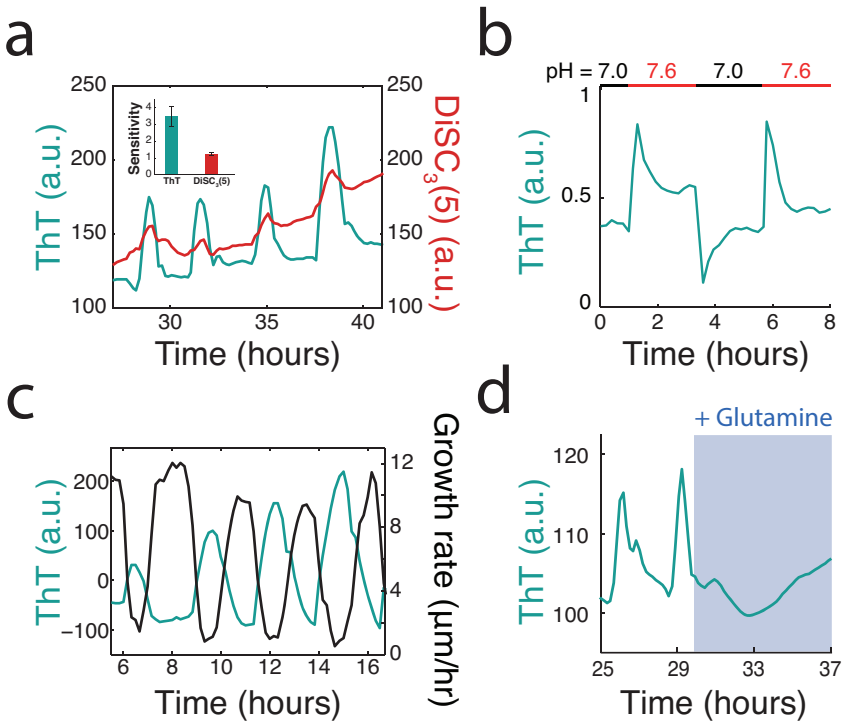

Extended Data Figure 1 | Thioflavin T (ThT) is a fluorescent reporter that is inversely related to the membrane potential. **a**, ThT and $DiSC_3(5)$, an established reporter of membrane potential in bacteria[23], both oscillate within biofilms. ThT has an approximately three fold higher sensitivity to changes in membrane potential compared to $DiSC_3(5)$. Sensitivity is defined as the ratio between peak height and error in peak height. Error bars indicate mean ± s.d. ($n = 8$ biofilm regions, averaged over the 4 pulses shown). **b**, The cellular ThT fluorescence depends on the external pH, where higher pH results in greater membrane potential, as expected[24]. ThT itself is insensitive to these pH changes and the traces are background subtracted to eliminate possible artefacts. Representative trace is selected from three independent biofilms. **c**, Oscillations in ThT and growth rate are inversely correlated, linking membrane potential oscillations to the metabolic cycle which produces periodic growth pauses[18]. Growth rate is calculated by taking the derivative of biofilm radius over time (Supplementary Information). Representative trace is selected from over 75 independent biofilms. **d**, Replacing glutamate with 0.2% glutamine, which eliminates the need to take up glutamate or retain ammonium, quenches ThT oscillations. This further suggests that ThT oscillations are specific to the metabolic cycle involving glutamate and ammonium. A representative trace was selected from three independent experiments.

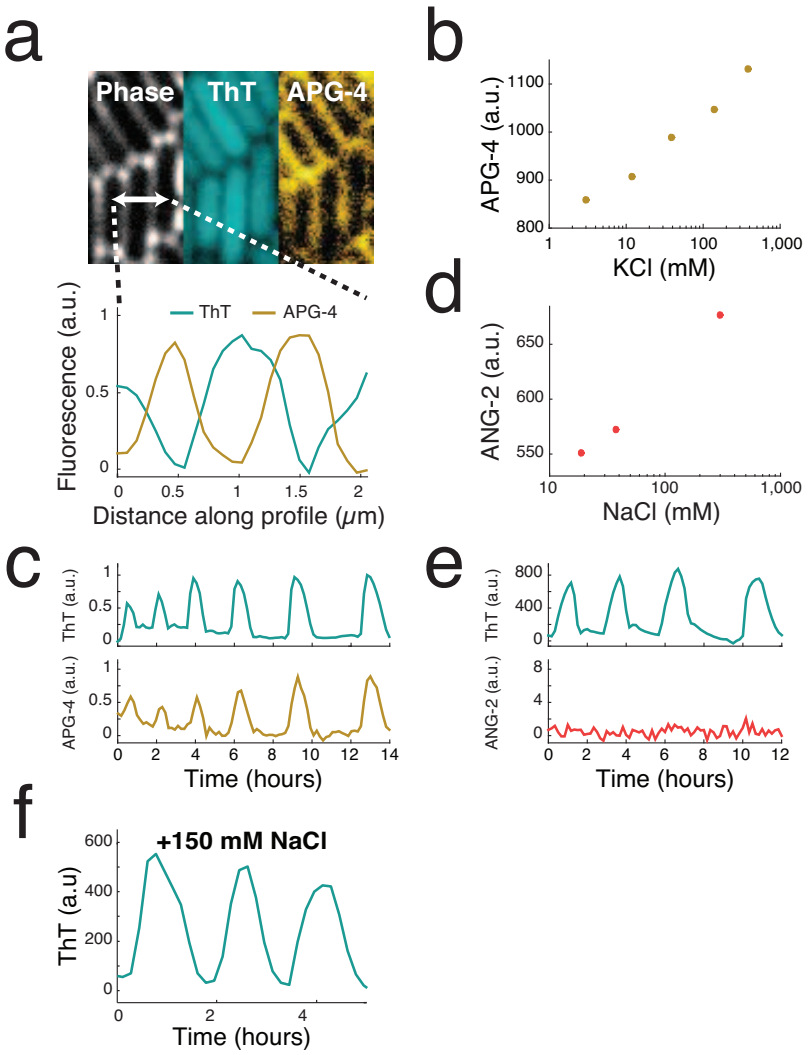

Extended Data Figure 2 | A fluorescent reporter of extracellular potassium (APG-4) indicates that potassium has a role in membrane potential oscillations. **a**, High-resolution images showing the intracellular localization of ThT and primarily extracellular localization of APG-4 (top). Quantification of ThT and APG-4 along the 2 μm profile indicated in the phase image indicates that APG-4 does not significantly diffuse into the cell (bottom). Representative images are selected from six independent experiments. **b**, Induction curve for APG-4 generated using externally supplemented KCl. The experiment was repeated twice. **c**, Oscillations in extracellular potassium in the surrounding cell-free region during biofilm oscillations. These oscillations occurred during the experiment shown in Fig. 2b, c and the pulses are synchronized between the biofilm and the surrounding cell-free region. Representative trace is selected from six independent experiments. **d**, Induction curve for ANG-2 generated using externally supplemented NaCl. The experiment was repeated twice. **e**, Simultaneous measurement of ThT and ANG-2 indicates a lack of oscillations in extracellular sodium. Representative trace selected from three independent biofilms. **f**, Furthermore, perturbing extracellular sodium concentrations in the media had no detectable effect on membrane potential oscillations. A representative trace was selected from four independent experiments.

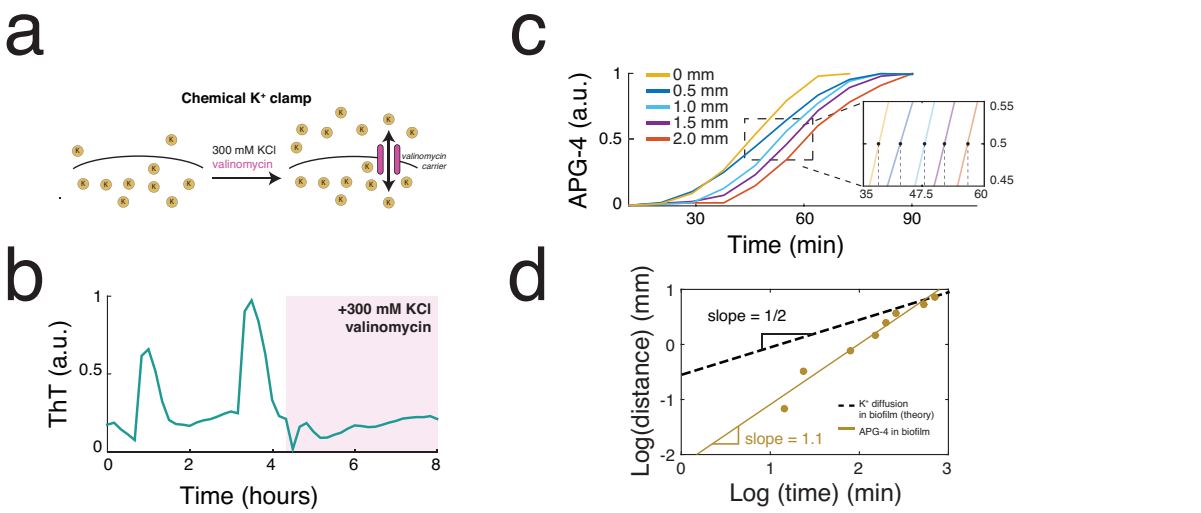

Extended Data Figure 3 | Active propagation of potassium signal within the biofilm. **a**, A chemical potassium clamp (300 mM KCl, matching the intracellular concentration[29], and 30 μM valinomycin) prevents the formation of potassium electrochemical gradients across the cellular membrane. Valinomycin is an antibiotic that creates potassium-specific carriers in the cellular membrane[32]. **b**, Clamping net potassium flux quenches oscillations in membrane potential. A representative trace was selected from two independent biofilms. **c**, Propagation of extracellular potassium is estimated by tracking the half-maximal position of the pulse over time. Representative traces are shown for a single pulse selected from one of six independent experiments. **d**, Propagation of extracellular potassium is relatively constant over time in contrast to diffusion that is expected to decay. The diffusion line is calculated using the mean squared displacement (MSD) and the diffusion coefficient for potassium in biofilms (Supplementary Information). Slopes are calculated from the same representative data shown in **c**.

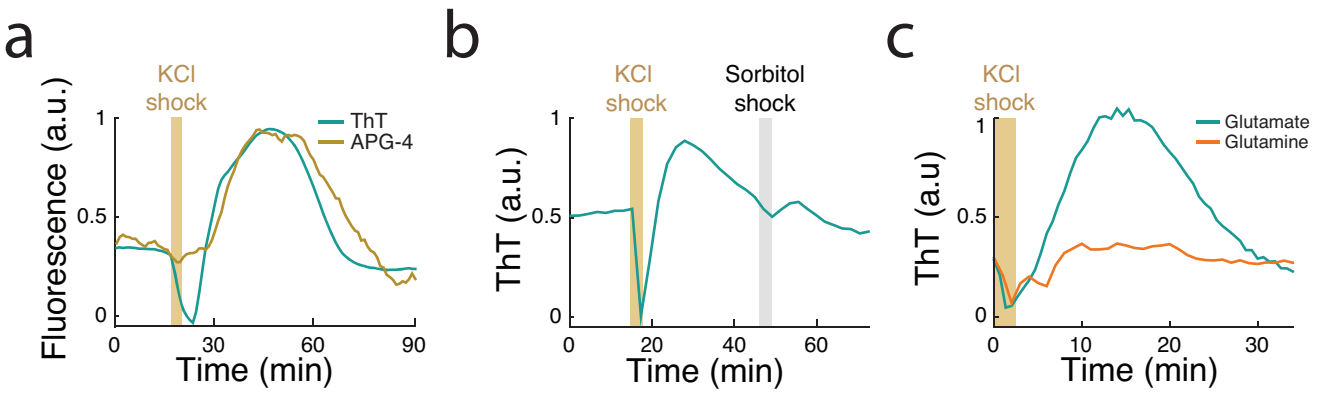

Extended Data Figure 4 | External potassium affects the metabolic state of the cell. **a**, A potassium shock (300 mM KCl) produces an initial ThT decrease (depolarization) followed by a period of sustained ThT increase (hyperpolarization). ThT is inversely related to the membrane potential. A corresponding pulse in APG-4 during this ThT increase suggests that hyperpolarization is due to release of potassium. APG-4 signal due to the external potassium shock itself was subtracted using the cell-free background near the biofilm. A representative trace was selected from three independent experiments. **b**, ThT spikes in response to external potassium shock (300 mM KCl) but not an equivalent shock of 300 mM sorbitol, an uncharged solute. A representative trace was selected from three independent experiments. **c**, The hyperpolarization response occurs when cells are grown in glutamate but not when glutamate is replaced by 0.2% glutamine, which bypasses the need to take up glutamate or retain ammonium. A representative trace was selected from four independent biofilms.

Extended Data Table 1 | List of strains used in this study

Strain	Genotype	Source
Wild type	*B. subtilis* NCIB 3610	*1*
ΔyugO	*yugO::* neo	This study
yugOΔtrkA	*trkA::* neo	This study

Extended Data Table 2 | Parameter values used in the model

Parameter	Value
g_K	30 min^{-1}
g_L	0.2 min^{-1}
V_{K0}	-380 mV
V_{L0}	-156 mV
S_{th}	40 μM
V_{th}	-150 mV
α_0	2 min^{-1}
β	1.3 min^{-1}
m	1
F	5.6 mM/mV

Parameter	Value
σ	0.2 mV
δ_K	1 mV/mM
δ_L	8 mV/mM
γ_s	0.1 min^{-1}
γ_e	10 min^{-1}
γ_t	4 min^{-1}
α_s	1 μM/(min mV)
α_t	1 μM/(min mV)
D	13.8×10^{-6} cm^2/s